Journal of Materials Chemistry C

ROYAL SOCIETY OF CHEMISTRY

PAPER

View Article Online
View Journal

Cite this: DOI: 10.1039/d6tc00714g

Unveiling the full configurational landscape of chiral phenanthrene-bridged diarylethene

Elias Djanffar,[ab] Violette Gousseau,[a] Muriel Escadeillas,[a] Nicolas Vanthuyne,[c] Marie Cordier,[a] Thierry Roisnel,[a] Elsa Caytan,[a] Arnaud Fihey,*[a] Rémi Dessapt*[b] and Julien Boixel*[a]

Received 6th March 2026,
Accepted 23rd March 2026

DOI: 10.1039/d6tc00714g

rsc.li/materials-c

We report the first complete experimental resolution of the configurational landscape of a phenanthrene-bridged diarylethene (DAE) with unsymmetrical substitution. Four stereoisomers—two antiparallel and two parallel—were isolated and fully characterized by chiral HPLC, circular dichroism, NMR, and single-crystal X-ray diffraction. This study demonstrates that parallel conformers, previously assumed to exist as a single *meso* form, are in fact distinct enantiomeric pairs. Thermal and kinetic analyses show that antiparallel conformers are both energetically favored and longer-lived, with racemization half-lives of up to one week at room temperature. The photochromic behavior of the phenanthrene-bridged DAE has been investigated in solution and in different condensed phases. In a PMMA matrix, and in the crystalline state, the closed antiparallel form displays significantly enhanced thermal stability at room temperature. These results uncover a previously unexplored stereochemical dimension in DAE chemistry, providing new avenues for the rational design of intrinsically chiral photochromic switches.

Introduction

Chirality is a defining feature of molecular systems, underpinning asymmetric catalysis, stereoselective recognition, and the development of functional material design.[1,2] In recent years, it has been increasingly integrated into photoresponsive frameworks, enabling dynamic systems in which stereochemical control couples with light-driven switching.[3]

Among photochromic scaffolds, diarylethenes (DAEs) stand out for their exceptional thermal stability, high photoconversion efficiency, and fatigue resistance,[4] properties that have secured their role in molecular electronics, data storage, and photonic devices. DAEs undergo conrotatory photocyclization and disrotatory photocycloreversion reactions that interconvert their open and closed isomers. The open form can adopt two distinct conformations – anti-parallel and parallel – but only the anti-parallel arrangement possesses the requisite orbital alignment for the conrotatory ring-closing reaction. In contrast, the parallel conformer is photochemically inert due to the misorientation of its reactive π-orbitals. The photoactive anti-parallel conformer exists as a pair of enantiomers (*R*,*S* and *S*,*R*) that, in most DAEs, rapidly interconvert thermally in solution. This dynamic equilibrium leads to racemization in the open form, ensuring that upon photocyclization, the resulting closed-ring isomers – bearing two stereogenic carbons and corresponding to the (*R*,*R*) and (*S*,*S*) enantiomers – are produced in equal proportions. Even the introduction of stereogenic substituents seldom perturbs this intrinsic stereochemical symmetry. To overcome this limitation and impart chirality to DAEs, restrictive chiral environments such as metallacycles,[5–7] cucurbituril or cyclodextrin inclusion complexes,[8,9] chiral dopants in liquid-crystals[10] and gels,[11] or covalent architectures including binaphthyl,[12] imine-bearing DTEs[13] or constrain on the reactive carbons[14–20] have been employed. These strategies can induce diastereoselective photocyclization[21] and measurable chiroptical responses, but do not create molecular switches that are intrinsically chiral at the DTE core. Consequently, systematic investigation of configurational isomers and their impact on light-driven reactivity has remained elusive.

Atropisomerism in DAEs – the hindered interconversion between parallel and anti-parallel DAE conformations – offers a unique handle for stereocontrol. Feringa *et al.* demonstrated that a phenanthrene-bridged DAE ($\Delta G \approx 110$ kJ mol^{-1}),[22] and Zhu *et al.* a benzothiadiazole analogue ($\Delta G \approx 140$ kJ mol^{-1})[23–25] could be conformationally immobilized by steric congestion, enabling enantioselective separation of atropisomers. Since then, intrinsic chirality in DAEs has been leveraged to enhance photo-quantum yields,[26,27] transduce mechanical force,[28,29]

[a] *Univ Rennes, CNRS, ISCR – UMR 6226, F-35000 Rennes, France. E-mail: julien.boixel@univ-rennes.fr*
[b] *Nantes Université, CNRS, IMN – UMR 6502, F-44000 Nantes, France. E-mail: Remi.Dessapt@cnrs-imn.fr*
[c] *Aix Marseille Université, UAR 1739 – Service 432, 13397 Marseille, France*

drive enantio-selective C–H activation,[30] and dictate (supra)-molecular helicity.[27,31]

The two anti-parallel conformers are well established as the photoactive forms, typically described by *M*/*P* or *R*,*R*/*S*,*S* stereo descriptors depending on substitution. In contrast, the parallel arrangement has consistently been regarded as a single *meso* form. However, computational studies on atropisomeric DAEs bearing sterically demanding phenanthrene bridges indicate that two distinct parallel conformers are theoretically accessible.[32] Despite decades of effort and multiple works indicating a 1 : 1 equilibria between anti-parallel and parallel populations, these two parallel isomers have never been experimentally resolved or structurally characterized.

The persistent description of the parallel conformer as a single *meso* form can be rationalized by both kinetic and structural factors. In most classical perfluorinated-bridged DAEs, the rotational barriers around the aryl–aryl bonds are insufficient to freeze atropisomerism at room temperature, leading to rapid interconversion of parallel conformations on the NMR timescale. Moreover, the frequent use of symmetrical substitution patterns provides no stereochemical bias capable of differentiating two parallel atropisomers experimentally. Even in sterically congested systems, chromatographic resolution of the parallel conformers has remained elusive, and crystallographic isolation has never been achieved. As a result, although theoretical studies predicted the possible existence of two distinct parallel arrangements, these were dynamically averaged or experimentally inaccessible, reinforcing the long-standing assumption of a single *meso* species.

In contrast, we report a phenanthrene-bridged DAE **1** specifically engineered with unsymmetrical substitution, that for the first time enables the experimental isolation and full characterization of all four configurational isomers: two anti-parallel and two parallel. Compound **1** combines three key structural features that collectively enable the experimental resolution of all four configurational isomers: (i) the rigid phenanthrene bridge, which significantly increases the rotational barrier; (ii) unsymmetrical substitution of the thiophene units, introducing stereochemical differentiation; and (iii) substantial steric congestion at the atropisomeric axis. This combination simultaneously freezes conformational interconversion and prevents dynamic averaging, thereby allowing chromatographic separation and crystallographic characterization of the two parallel enantiomers. The present system thus reveals that the parallel conformer, long regarded as a single *meso* species, is in fact an unresolved enantiomeric pair. This unprecedented degree of structural control represents a breakthrough in the design of chiral DAEs systems and opens an unexplored dimension for the rational design of intrinsically chiral photochromic systems.

Results and discussion

Synthesis and characterization

The synthetic strategy toward compound **1**, detailed in SI, is inspired by the work of Kawai *et al.*, who constructed a helicene-bridged DTE *via* a Suzuki cross-coupling reaction.[27] However, the dissymmetric nature of the target compound **1** necessitates a stepwise construction of the DTE backbone *via* intermediate **2**, using successive Suzuki–Miyaura cross-coupling reactions involving individually prepared thiophene boronic ester units (**3** and **4**), and the non-commercially available dibromophenanthrene **5** (Scheme 1 and Fig. S1–S4, SI). The key intermediate **5** was synthesized according to the procedure reported by Mansø *et al.*[33] The first Suzuki–Miyaura coupling was performed with the 2,5-dimethylthiophene boronic derivative **3**, as attempts to start with the 2-pyridyl analogue **4** resulted in very low yields.

^{1}H and ^{13}C NMR spectra of **1** display two signal sets indicative of a diastereotopic relationship; through-space correlations support their assignment to diastereomers corresponding to the anti-parallel and parallel conformers (Fig. S5 and S6, SI). The stereoisomers of **1** were separated by chiral HPLC and characterized by ^{1}H NOESY and ^{13}C NMR spectrophotometry (Fig. S7–S10, SI and Table S1, SI). Two pairs of enantiomers were isolated, two parallel forms (hereafter labeled as $\mathbf{1p_1}$ and $\mathbf{1p_2}$), and two anti-parallel ones (hereafter labeled as $\mathbf{1o_{(S)}}$ and $\mathbf{1o_{(R)}}$).

Suitable single crystals of each parallel enantiomer ($\mathbf{1p_1}$ and $\mathbf{1p_2}$), and of a racemic mixture of antiparallel enantiomers ($\mathbf{1o_{(S)}}$/$\mathbf{1o_{(R)}}$) have been successfully obtained by slow evaporation of a concentrated acetonitrile-dichloromethane solution (SI). The crystal structures of the three compounds have been determined by single-crystal X-ray diffraction (SCXRD) (Table S2, SI), allowing us to unambiguously clarify the chirality of the stereoisomers. The ORTEP views of the $\mathbf{1o_{(S)}}$/$\mathbf{1o_{(R)}}$ racemic mixture, $\mathbf{1p_1}$ and $\mathbf{1p_2}$ are presented in Fig. 1. $\mathbf{1o_{(S)}}$/$\mathbf{1o_{(R)}}$ crystallizes in the centrosymmetric $P2_1/n$ space group (Table S2, SI). As expected, the crystal structure contains a racemic mixture of the chiral $\mathbf{1o_{(S)}}$ and $\mathbf{1o_{(R)}}$ enantiomers (Fig. 1a) which exhibit the antiparallel conformation. In both molecules, the phenanthrene bridge deviates slightly from planarity, with a torsion angle of 3.5(4)° between its two aromatic rings. By comparison, the precursor **5** exhibits an almost planar phenanthrene moiety with a torsion angle of 1.2°.[34] This increase in the torsion angle of the phenanthrene bridge can be attributed to the steric constraints imposed by the atropisomerism with the thiophene rings. The C9···C28 distance between the reactive carbons is of 4.548(4) Å. Although this distance appears relatively long compared to those typically observed for classical perfluorinated-bridged DAEs,[35] it remains shorter than the values reported for related phenanthrene-bridged DAEs.[36] The $\mathbf{1o_{(S)}}$ and $\mathbf{1o_{(R)}}$ enantiomers are arranged into supramolecular head-to-tail dimers along the *b*–axis (Fig. S11, SI), the shortest intermolecular S2···S2

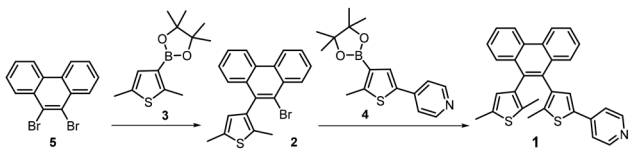

Scheme 1 Stepwise synthetic access to **1**.

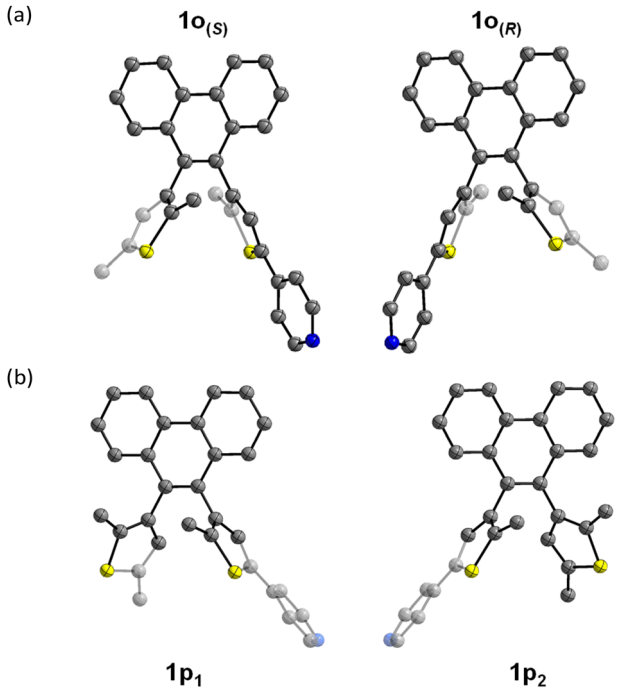

Fig. 1 ORTEP representations of the molecular structures of (a) **1o$_{(R)}$** and **1o$_{(S)}$** anti-parallel enantiomers in the racemic mixture **1o$_{(S)}$**/**1o$_{(R)}$**, and (b) **1p$_1$** and **1p$_2$** parallel enantiomers, with thermal ellipsoids at 50% probability.

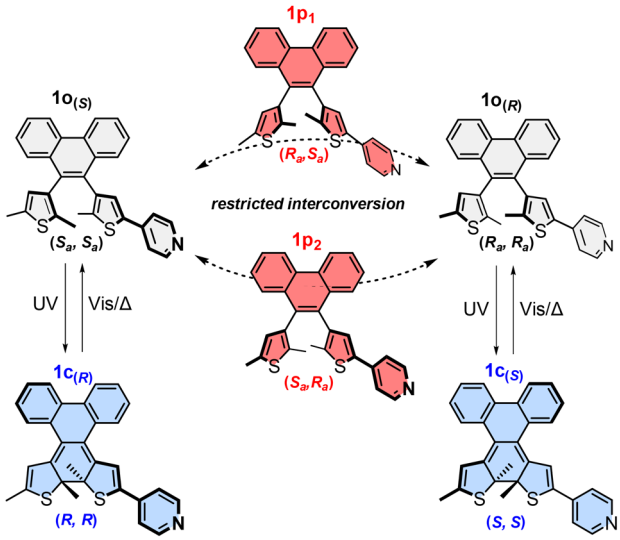

Chart 1 Scheme of the different isomers of **1** and their relative conversion pathways.

distance being of 3.6921(17) Å. Nevertheless, no intermolecular π···π stacking interactions involving the phenanthrene or pyridine groups are observed.

Enantiopure **1p$_1$** and **1p$_2$** molecules crystallize in the chiral Sohncke space groups $P3_2$ and $P3_1$, respectively (Table S2, SI). The two enantiomers exhibit a clear designable parallel conformation (Fig. 1b). As observed for **1o$_{(S)}$** and **1o$_{(R)}$**, the phenanthrene bridge of **1p$_1$** and **1p$_2$** shows a slight distortion with a torsion angle of 4.6(3)° for **1p$_1$** and −4.5(4)° for **1p$_2$**. The **1p$_1$** and **1p$_2$** molecules are arranged into supramolecular left-handed and right-handed helices, respectively, running along the *c*-axis (Fig. S12, SI), so that the shortest intermolecular S1···S1 distance is of 3.6890(4) Å for **1p$_1$**, and of 3.6873(6) Å for **1p$_2$** (Fig. S13, SI), both of them being very close to that observed in the crystal structure of **1o$_{(S)}$**/**1o$_{(R)}$**. Neither the phenanthrene groups nor the pyridine unit are involved in intermolecular π···π stacking interactions.

The chirality of related phenanthrene- or benzothiadiazole-bridged DTEs is most often described using *P* and *M* helicity descriptors. However, in the case of compound **1**, we found it difficult to assign such helicity-based descriptors when examining the resolved crystal structures. Instead, the absolute configuration of the four open-form isomers of **1** was determined based on their atropisomeric axes, using the R_a or S_a notation (Fig. S14, SI). For the closed-form isomers, chirality is typically defined by the stereochemistry at the reactive carbon centers (Chart 1).

As expected, upon UV-light irradiation at 330 nm, the pair of anti-parallel isomers **1o$_{(S)}$** and **1o$_{(R)}$** display photochromic behavior in diluted dichloromethane solution at 298 K, while **1p$_1$** and **1p$_2$** are unresponsive under similar UV-light exposure. Before photoexcitation, the electronic absorption spectra of the antiparallel **1o$_{(S)}$** isomer (Fig. 2a) and the parallel **1p$_1$** isomer (Fig. 2b) are very similar, displaying transitions exclusively in the UV region (Table S3, SI). Notably, the same conclusion holds when comparing **1o$_{(R)}$** and **1p$_2$**: each pair of isomers exhibits identical absorption features. The computed TD-DFT electronic transitions (see SI) reflect these observations, resulting in nearly identical absorption spectra for antiparallel and parallel isomers (Fig. S31, SI and Table S4, SI), despite a notable difference in the topology of the first excited state which is DTE-centered for the former with a non-negligible intensity while it

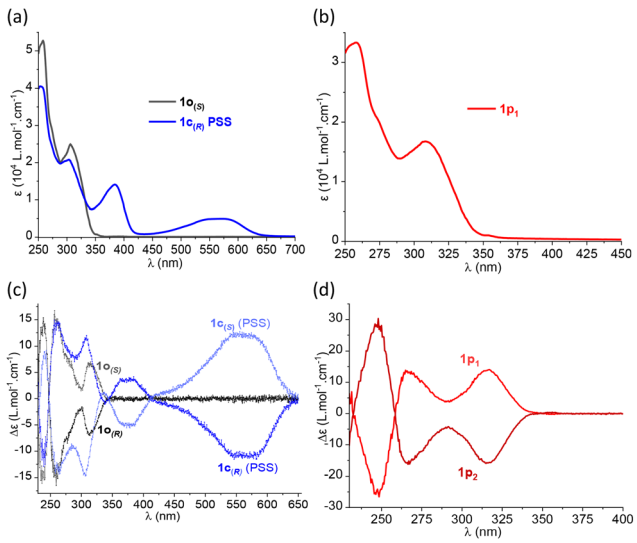

Fig. 2 Absorbance spectra of (a) **1o$_{(S)}$**, before and after 330 nm-light irradiation, and (b) **1p$_1$** in dichloromethane at 298 K ($C \approx 10^{-6}$ M). Circular dichroism spectra of (c) **1o$_{(S)}$** and **1o$_{(R)}$**, before and after 330 nm-light irradiation, and (d) **1p$_1$** and **1p$_2$** in dichloromethane at 298 K ($C \approx 10^{-3}$ M).

presents a charge transfer character for the latter, with a vanishing intensity (Fig. S33 and S34, SI).

Upon UV-light irradiation at 330 nm, the racemic mixture of **1o**$_{(S)}$ and **1o**$_{(R)}$ progressively turns form colourless to purple. The colour change deals with the appearance of a broad absorption band that grows up in the visible region (450–650 nm, $\lambda_{max} \approx 560$ nm), along with a narrower higher-energy band in the 350–420 nm range ($\lambda_{max} \approx 385$ nm) (Fig. 2a). The first absorption band is attributed to the computed $S_0 \rightarrow S_1$ transition, and the second one to the $S_0 \rightarrow S_3$ transition (Table S4, SI and Fig. S32, SI). Both transitions show a high degree of electronic delocalization along the DTE and the phenanthrene moieties (Fig. S35, SI). Light-irradiation at wavelengths above 450 nm leads to full recovery of the initial absorption spectra, and the compounds demonstrate reasonable fatigue resistance over 10 open/close photochromic cycles (Fig. S15, SI). As previously reported, phenanthrene-bridged DTEs are prone to photodegradation under prolonged UV-light exposure, particularly at wavelengths below 300 nm.[37]

Compared to their perfluorinated counterparts, phenanthrene-bridged DAEs are markedly more susceptible to thermally driven cycloreversion.[36,37] The thermal stability of **1c** was assessed in the PSS state on a racemic mixture of anti-parallel closed-ring isomers by monitoring cycloreversion kinetics over a temperature range (Fig. 3a). Selective detection at 560 nm revealed a clean mono-exponential decay, enabling extraction of rate constants. Arrhenius analysis (Fig. 3b) yielded an activation barrier of 74 kJ mol^{-1}, indicating only moderate energetic requirements for bond reorganization. The closed-ring form **1c** exhibits a half-life of 10.6 min at 293 K in solution ($k_{th}^{293} = 1.1 \times 10^{-3}$ s^{-1}), underscoring its fleeting stability under ambient conditions.

Experimental and computational studies consistently show that electron-withdrawing substituents destabilize the closed form of perfluorinated-bridged DAEs by depleting electron density on the conjugated core, thereby accelerating thermal cycloreversion.[4,38] A similar effect is observed in phenanthrene-bridged DAEs, accounting for the short half-life of **1c**.[39,40] Based on this, the open-to-closed conversion yield, measured by ^{1}H NMR, reaches 80% at 253 K, minimizing thermal cycloreversion (Fig. S16, SI). Bleaching at 293 K through time leads to fully recovered open form (Fig. S17, SI). The quantum yields of cyclization ($\varnothing_{o\rightarrow c}^{330}$) and cycloreversion ($\varnothing_{c\rightarrow o}^{580}$) reactions for **1o**$_{(S)}$/**1c**$_{(R)}$ and **1o**$_{(R)}$/**1c**$_{(S)}$ were determined at 330 and 580 nm, respectively. The temperature was maintained at 283 K during the recording of the kinetics to minimize the impact of the thermal cycloreversion (Fig. S18, SI). The high photocyclization quantum yields, $\varnothing_{o\rightarrow c}^{330}$ of 0.956 (**1o**$_{(S)}$ → **1c**$_{(R)}$) and 0.965 (**1o**$_{(R)}$ → **1c**$_{(S)}$), are consistent with the exclusive photoreactivity of the antiparallel isomers, as previously reported for benzothiadiazole-bridged DTEs.[25,41] Conversely, the photocycloreversion yields $\varnothing_{c\rightarrow o}^{580}$ of 0.096 (**1c**$_{(R)}$ → **1o**$_{(S)}$) and 0.102 (**1c**$_{(S)}$ → **1o**$_{(R)}$) are higher than those observed for related systems. This behavior is consistent with the presence of the electron-withdrawing pyridine group, which is known to facilitate the ring-opening process in DTEs.[36]

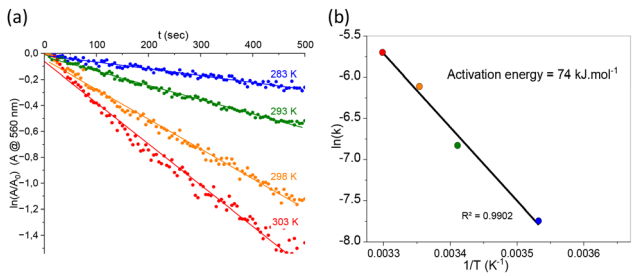

Fig. 3 (a) Kinetics of the thermal cycloreversion of **1c** at λ_{max} = 560 nm. (b) Resulting Arrhenius analysis.

Circular dichroism (CD) spectra of **1o**$_{(S)}$ and **1o**$_{(R)}$ (Fig. 2c), and **1p$_1$** and **1p$_2$** (Fig. 2d) confirm the chiroptical activity of each isolated isomer, and reveal for each pair of molecules two enantiomeric signals opposite at all wavelengths. Unlike UV-Vis spectra, clear differences are observable between open anti-parallel (**1o**$_{(S)}$/**1o**$_{(R)}$) and parallel (**1p$_1$**/**1p$_2$**) configurations. The **1p$_1$** and **1p$_2$** isomers display a single-sign band between 230–260 nm, whereas the **1o**$_{(S)}$ and **1o**$_{(R)}$ forms exhibit exciton-coupled features. TD-DFT calculations reproduce both the sign and position of the CD signals, as well as the relative intensity of the bands (Fig. S31 and S32, SI). Photochromic cycles conducted on **1o**$_{(S)}$ and **1o**$_{(R)}$, upon alternative irradiation at 340 and 540 nm, demonstrate that chirality is fully retained during both photocyclization and cycloreversion reactions (Fig. 2c).

The room-temperature photochromic properties of **1** in condensed phases have been also investigated. First, embedded in a PMMA film (doping rate: 5% in weight, see SI for the detailed preparation procedure), the racemic mixture **1o**$_{(S)}$/**1o**$_{(R)}$ preserves full switching ability when exposed to UV-light irradiation (λ_{ex} = 300 nm) (Fig. S19, SI). When maintaining the resulting purple film into darkness, the photogenerated absorption band at λ_{max} = 570 nm exhibits a negligible loss in intensity. However, this band fully disappears by exposing the film onto visible-light irradiation (λ_{ex} = 590 nm) for 30 min, which indicates the complete recovering of the open-ring **1o**$_{(S)}$/**1o**$_{(R)}$ isomers in the PMMA matrix. Noticeably, the pure microcrystalline powder of **1o**$_{(S)}$/**1o**$_{(R)}$ also exhibits photochromic activity upon UV-light excitation (λ_{ex} = 305 nm) at room temperature (Fig. S20, SI), and the color of the powdered sample gradually shifts from white to purple. The absorption band of the closed-ring **1c** isomers at λ_{max} = 560 nm increases in intensity with irradiation time, and the PSS is almost reached after 10 min (Fig. S21, SI). These well evidences that the photocyclization of the **1o**$_{(S)}$ and **1o**$_{(R)}$ isomers is active in the crystalline state, despite a relatively long intermolecular distance between the two reactive carbon atoms (see above). This is also in good agreement with the lack of intermolecular π···π stacking interactions between the **1o** molecules in the crystal lattice of **1o**$_{(S)}$/**1o**$_{(R)}$ that could dramatically restrict their photoconversion. However, due to their close proximity in the molecular crystal structure, the **1c** isomers are further stabilized in the

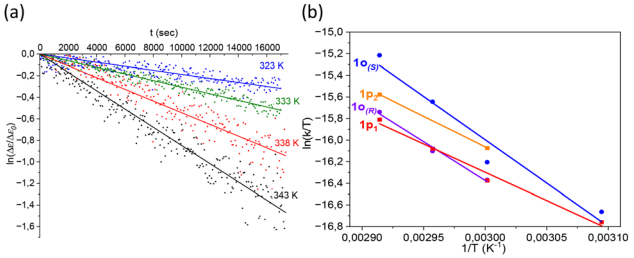

Fig. 4 Racemization of stereoisomers: (a) CD decay of $\mathbf{1o_{(S)}}$ in 1,2-dichloroethane at various temperatures, yielding rate constants k_{rn}; (b) Eyring plots used to extract activation energies.

crystalline state than in diluted dichloromethane solution. Thus, the thermally driven cycloreversion process at 293 K is markedly slowed down in the powder of $\mathbf{1o_{(S)}}/\mathbf{1o_{(R)}}$, extending the half-life of **1c** to 110 min (Fig. S22, SI), an order of magnitude longer than in solution (10.6 min). As already observed for other powder samples of DAEs,[42,43] the absorption band of **1c** does not totally disappear even after a long period of almost 1 day, indicating that a part of the closed-ring isomers remains stabilized in the bulk solid.

The interconversion processes between the anti-parallel and parallel enantiomers (Chart 1), have been investigated by VT-NMR experiments at 340, 350 and 360 K (Fig. S23–S25, SI). Starting from the enantiomeric pair $\mathbf{1o_{(S)}}/\mathbf{1o_{(R)}}$ and assuming a first-order kinetic law, the racemization half-life is estimated from on a Eyring plot, and extrapolation to 298 K afforded an activation energy (AE) of 106 kJ mol^{-1} (Fig. S26, SI). The same set of NMR experiment has been conducted with the parallel enantiomeric pair $\mathbf{1p_1}/\mathbf{1p_2}$, yielding to comparable activation energy of 108 kJ mol^{-1} (Fig. S26, SI). DFT energy difference between the relaxed structure of the antiparallel and parallel conformers is found to favor the former by only 0.2 kJ mol^{-1}, indicating that the conformers are essentially isoenergetic, as such a small difference falls within DFT accuracy limit (the two enantiomers of a given conformation are found perfectly isoenergetic, SI). However, the racemization process appears to proceed symmetrically, regardless of which enantiopure compound is used as the starting material; for example, $k(\mathbf{1o_{(R)}} \rightarrow \mathbf{1p_2}) \approx k(\mathbf{1o_{(R)}} \rightarrow \mathbf{1p_1})$ and $k(\mathbf{1p_1} \rightarrow \mathbf{1o_{(S)}}) \approx k(\mathbf{1p_1} \rightarrow \mathbf{1o_{(R)}})$. Computed DFT energy barrier between parallel and antiparallel conformers (Table S5, SI) are in very good quantitative agreement with the VT-NMR experiments, all values lying in the 100 to 130 kJ mol^{-1} range, pinpointing thus also toward a symmetric behavior. In this energy range, the difference in the computed barriers is indeed deemed as non-characteristic or at least cannot be easily correlated to the complex experimental setup, given the simplistic character of the DFT protocol (energy scan on an isolated molecule, without temperature and dynamical effect).

The apparent isoenergetic nature of the interconversion pathways justifies the application of a first-order kinetic model to assess the stability of each individual enantiomer. Accordingly, the temporal retention of chirality for each enantiomer was systematically monitored. The decay of the variation of absorbance signal (ΔA) of circular dichroism provided racemization rate constants (k_{rn}), from which activation energies and half-lives were derived assuming first order kinetic law (Fig. 4a, Table 1). As an example, for the stereoisomer $\mathbf{1o_{(S)}}$, linear fits of $\ln(\Delta A/\Delta A_0)$ *vs* time at 343–323 K yielded rate constants that decrease with temperature, consistently with slower racemization at lower temperatures (Fig. 4a). While values slightly differ between enantiomers, each shows internal consistency across temperatures (Fig. S27–S29, SI). Eyring analysis gave activation energies, with $\mathbf{1o_{(S)}}/\mathbf{1o_{(R)}}$ stereoisomers consistently higher than $\mathbf{1p_1}/\mathbf{1p_2}$ stereoisomers, reflecting the greater stability against racemization of anti-parallel conformers (Fig. 4b, Table 1). Interestingly, this enhanced stability in favor of the anti-parallel enantiomers, evidenced by means of chiroptical measurements is in line with the anti-parallel enrichment observed by ^{1}H-NMR (Fig. S23–S25, SI).

Table 1 Activation energies at 273 K obtained from Eyring analysis

Enantiomer	Activation energy at 273 K (kJ mol^{-1})
$\mathbf{1o_{(S)}}$	102.3
$\mathbf{1o_{(R)}}$	101.9
$\mathbf{1p_1}$	98.8
$\mathbf{1p_2}$	96.9

Conclusion

We have unveiled the full configurational landscape of a phenanthrene-bridged diarylethene, isolating and structurally characterizing for the first time all four stereoisomers: two antiparallel and two parallel. Beyond the structural elucidation of a single molecular example, this work establishes experimentally that the parallel conformer, long treated as a single *meso* entity in diarylethene chemistry, actually exists as two distinct enantiomers. This finding revises the stereochemical description of DAEs that has prevailed for more than three decades, and demonstrates that the open form of atropisomeric diarylethenes inherently comprises four configurational isomers rather than three.

Their absolute configurations have been unambiguously resolved by single-crystal X-ray diffraction and NMR spectroscopy. Comprehensive photophysical studies in solution and in condensed phases confirm robust photochromism for the antiparallel isomers, while the parallel ones remain photoinactive. Thermal and kinetic analyses reveal that (i) the interconversion processes $\mathbf{1o} \rightarrow \mathbf{1p}$ and $\mathbf{1p} \rightarrow \mathbf{1o}$ occur isoenergetically through enantiomeric pathways, and (ii) antiparallel enantiomers are both more stable and longer-lived than their parallel counterparts against racemization. Remarkably, despite the presence of the electron-withdrawing pyridyl substituent, the closed-ring **1c** form exhibits strongly improved thermal stability in the crystalline state or when embedded in a PMMA film.

By experimentally demonstrating the existence and isolability of both parallel atropisomers, this study uncovers a previously unrecognized stereochemical dimension in diarylethene chemistry. It therefore provides a conceptual framework

for the rational design of intrinsically chiral photochromic switches in which configurational control extends beyond the classical antiparallel/parallel dichotomy.

This discovery provides the first direct evidence for the existence of both parallel atropisomers, overturning a long-standing assumption in DAE chemistry. It represents a decisive advance in the stereochemical understanding of these molecular switches, and opens an entirely new dimension in the design of intrinsically chiral, light-responsive molecular systems.

Conflicts of interest

There are no conflicts to declare.

Data availability

The supporting data has been provided as part of the supplementary information (SI). Supplementary information: Tables S1–S5, NMR spectra Figure S1–S9 and further experimental details (chiral chromatography separation, additional photophysical data, VT-NMR study, additional kinetic data – temporal retention of chirality and additional theoretical data). See DOI: https://doi.org/10.1039/d6tc00714g.

CCDC 2517058–2517060 contain the supplementary crystallographic data for this paper.[44a–c]

Acknowledgements

This work received financial support from the CNRS, the University of Rennes, Nantes Université, the Ministère de l'Enseignement Supérieur et de la Recherche, and ANR for Financial support *via* EUR LUMOMAT Project. Part of this work has been performed using the PRISM core facility (Biogenouest, Univ Rennes, Univ Angers, INRAE, CNRS, FRANCE). Certain optical measurements were performed using the IMN's characterization platform, PLASSMAT, Nantes, France. The authors are grateful to the analytical center CRMPO for the elemental and HRMS analyses.

References

1 J. K. Cheng, S.-H. Xiang, S. Li, L. Ye and B. Tan, *Chem. Rev.*, 2021, **121**, 4805–4902.
2 W. Cai, X. Xie, Z. Yang and X. Guo, *Angew. Chem., Int. Ed.*, 2025, **64**, e202504558.
3 T. Ooi, *Science*, 2011, **331**, 1395–1396.
4 M. Irie, T. Fukaminato, K. Matsuda and S. Kobatake, *Chem. Rev.*, 2014, **114**, 12174–12277.
5 Y.-X. Wang, Q.-F. Zhou, S.-T. Jiang, Y. Zhang, G.-Q. Yin, B. Jiang, X. Li, H. Tan and H.-B. Yang, *Macromol. Rapid Commun.*, 2018, **39**, 1800454.
6 S. Guo, M. Li, H. Hu, T. Xu, H. Xi and W.-H. Zhu, *Chem. Sci.*, 2023, **14**, 6237–6243.
7 G. Shaomeng, L. Mengqi, L. Cheng, Z. Weiwei, H. Honglong, L. Ning and Z. Wei-Hong, *CCS Chem.*, 2024, **7**, 1005–1015.
8 G. Liu, C. Tian, X. Fan, X. Xue, L. Feng, C. Wang and Y. Liu, *JACS Au*, 2023, **3**, 2550–2556.
9 M. Takeshita, N. Kato, S. Kawauchi, T. Imase, J. Watanabe and M. Irie, *J. Org. Chem.*, 1998, **63**, 9306–9313.
10 Y. Wang and Q. Li, *Adv. Mater.*, 2012, **24**, 1926–1945.
11 Y. Cai, Z. Guo, J. Chen, W. Li, L. Zhong, Y. Gao, L. Jiang, L. Chi, H. Tian and W.-H. Zhu, *J. Am. Chem. Soc.*, 2016, **138**, 2219–2224.
12 Y. Li, M. Wang, H. Wang, A. Urbas and Q. Li, *Chem. – Eur. J.*, 2014, **20**, 16286–16292.
13 T. van Leeuwen, T. C. Pijper, J. Areephong, B. L. Feringa, W. R. Browne and N. Katsonis, *J. Mater. Chem.*, 2011, **21**, 3142–3146.
14 M. Kose, M. Shinoura, Y. Yokoyama and Y. Yokoyama, *J. Org. Chem.*, 2004, **69**, 8403–8406.
15 T. Okuyama, Y. Tani, K. Miyake and Y. Yokoyama, *J. Org. Chem.*, 2007, **72**, 1634–1638.
16 Y. Yokoyama, T. Shiozawa, Y. Tani and T. Ubukata, *Angew. Chem., Int. Ed.*, 2009, **48**, 4521–4523.
17 S. Delbaere, J. Berthet, T. Shiozawa and Y. Yokoyama, *J. Org. Chem.*, 2012, **77**, 1853–1859.
18 T. Shiozawa, M. K. Hossain, T. Ubukata and Y. Yokoyama, *Chem. Commun.*, 2010, **46**, 4785–4787.
19 Y. Tani, T. Ubukata, Y. Yokoyama and Y. Yokoyama, *J. Org. Chem.*, 2007, **72**, 1639–1644.
20 M. Takeshita and H. Jin-nouchi, *Chem. Commun.*, 2010, **46**, 3994–3995.
21 S. Yamamoto, K. Matsuda and M. Irie, *Org. Lett.*, 2003, **5**, 1769–1772.
22 M. Walko and B. L. Feringa, *Chem. Commun.*, 2007, 1745–1747.
23 W. Li, C. Jiao, X. Li, Y. Xie, K. Nakatani, H. Tian and W. Zhu, *Angew. Chem., Int. Ed.*, 2014, **53**, 4603–4607.
24 W. Li, Y. Cai, X. Li, H. Ågren, H. Tian and W.-H. Zhu, *J. Mater. Chem. C*, 2015, **3**, 8665–8674.
25 M. Li and W.-H. Zhu, *Acc. Chem. Res.*, 2022, **55**, 3136–3149.
26 M. Yamada, T. Sawazaki, M. Fujita, F. Asanoma, Y. Nishikawa and T. Kawai, *Chem. – Eur. J.*, 2022, **28**, e202201286.
27 R. Li, Q. Fang, M. Chen, M. Yamada, Y. Tsuji, Y. Kugai, W. Li and T. Kawai, *Chem. – Eur. J.*, 2023, **29**, e202302693.
28 X. Fu, B. Zhu and X. Hu, *J. Am. Chem. Soc.*, 2023, **145**, 15668–15673.
29 C. Zhang, T. B. Kouznetsova, B. Zhu, L. Sweeney, M. Lancer, I. Gitsov, S. L. Craig and X. Hu, *J. Am. Chem. Soc.*, 2025, **147**, 2502–2509.
30 G. Zhang, X. Wu, S. Mao, M. Li, H. Hu, B.-F. Shi and W.-H. Zhu, *Chem. Sci.*, 2024, **15**, 20013–20021.
31 J. Hou, J. Wang, A. Ryabchun and B. L. Feringa, *Adv. Funct. Mater.*, 2024, **34**, 2312831.
32 J. M. Cox, I. M. Walton and J. B. Benedict, *J. Mater. Chem. C*, 2016, **4**, 4028–4033.
33 M. Mansø, L. Fernandez, Z. Wang, K. Moth-Poulsen and M. B. Nielsen, *Molecules*, 2020, **25**, 322.

34 R. Yokota, C. Kitamura and T. Kawase, *Acta Crystallogr., Sect. E:Struct. Rep. Online*, 2012, **68**, o3174.
35 M. Irie, T. Fukaminato, K. Matsuda and S. Kobatake, *Chem. Rev.*, 2014, **114**, 12174–12277.
36 E. Chatir, M. Boggio-Pasqua, F. Loiseau, C. Philouze, G. Royal and S. Cobo, *Chem. – Eur. J.*, 2022, **28**, e202103755.
37 Q. Luo, S. Li, W. Ding, W. Lei, S. Gou and S. Chen, *Dyes Pigm.*, 2024, **224**, 112051.
38 Q. Ai, K. Lan, L. Li, Z. Liu and X. Hu, *Adv. Sci.*, 2024, **11**, 2410524.
39 J. He, T. Wang, S. Chen, R. Zheng, H. Chen, J. Li and H. Zeng, *J. Photochem. Photobiol., A*, 2014, **277**, 45–52.
40 Q. Luo, S. Li, W. Ding, W. Lei, S. Gou and S. Chen, *Dyes Pigm.*, 2024, **224**, 112051.
41 W. Li, C. Jiao, X. Li, Y. Xie, K. Nakatani, H. Tian and W. Zhu, *Angew. Chem., Int. Ed.*, 2014, **53**, 4603–4607.
42 P. Bolle, C. Menet, M. Puget, H. Serier-Brault, S. Katao, V. Guerchais, F. Boucher, T. Kawai, J. Boixel and R. Dessapt, *J. Mater. Chem. C*, 2021, **9**, 13072–13076.
43 O. Stetsiuk, P. Bolle, M. Cordier, J. Boixel and R. Dessapt, *J. Mater. Chem. C*, 2022, **10**, 899–907.
44 (*a*) CCDC 2517058: Experimental Crystal Structure Determination, 2026, DOI: 10.5517/ccdc.csd.cc2qh6fw; (*b*) CCDC 2517059: Experimental Crystal Structure Determination, 2026, DOI: 10.5517/ccdc.csd.cc2qh6gx; (*c*) CCDC 2517060: Experimental Crystal Structure Determination, 2026, DOI: 10.5517/ccdc.csd.cc2qh6hy.